

Learning Geometric Invariance for Gait Recognition

Zengbin Wang*, ^{ID} Junjie Li*, ^{ID} Saihui Hou^{† ID}, Member, IEEE, Xu Liu^{ID}, Chunshui Cao^{ID}, Yongzhen Huang^{ID}, Senior Member, IEEE, Muyi Sun^{ID}, Siye Wang^{ID}, Man Zhang^{‡ ID} Member, IEEE

Abstract—The goal of gait recognition is to extract identity-invariant features of an individual under various gait conditions, *e.g.*, cross-view and cross-clothing. Most gait models strive to implicitly learn the common traits across different gait conditions in a data-driven manner to pull different gait conditions closer for recognition. However, relatively few studies have explicitly explored the inherent relations between different gait conditions. For this purpose, we attempt to establish connections among different gait conditions and propose a new perspective to achieve gait recognition: variations in different gait conditions can be approximately viewed as a combination of geometric transformations. In this case, all we need is to *determine the types of geometric transformations and achieve geometric invariance, then identity invariance naturally follows*. As an initial attempt, we explore three common geometric transformations (*i.e.*, Reflect, Rotate, and Scale) and design a Reflect-Rotate-Scale invariance learning framework, named *RRS-Gait*. Specifically, it first flexibly adjusts the convolution kernel based on the specific geometric transformations to achieve approximate feature equivariance. Then these three equivariant-aware features are respectively fed into a global pooling operation for final invariance-aware learning. Extensive experiments on four popular gait datasets (Gait3D, GREW, CCPG, SUSTech1K) show superior performance across various gait conditions.

Index Terms—Gait Recognition, Geometric Transformation, Equivariance Learning, Invariance Learning

I. INTRODUCTION

Gait recognition, aiming to capture unique walking patterns of an individual, has become a promising biometric identification technology. Its primary advantage lies in the ability to perform recognition at a long distance without requiring cooperation from the individual [1], [2]. Recent progress [3]–[5] has demonstrated remarkable performance under various challenging conditions, such as cross-view and cross-clothing,

This work is jointly supported by the National Natural Science Foundation of China (62276031, 62276025, 62206022, 62476027), the National Key Research and Development Program of China (2023YFF0904700), the Doctoral Innovation Fund of Beijing University of Posts and Telecommunications (CX20242083), and the Fundamental Research Funds for the Central Universities (2253200026).

Zengbin Wang, Junjie Li, Muyi Sun, and Siye Wang are with School of Artificial Intelligence, Beijing University of Posts and Telecommunications, Beijing 100876, China. (Email: {wzb1, hnjj, muyi.sun, wsy}@bupt.edu.cn).

Man Zhang are with School of Artificial Intelligence, Beijing University of Posts and Telecommunications, and School of Computer and Information Science, Qinghai Institute of Technology. (Email: zhangman@bupt.edu.cn).

Saihui Hou and Yongzhen Huang are with the School of Artificial Intelligence, Beijing Normal University, Beijing 100875, China. (Email: {housaihui, huangyongzhen}@bnu.edu.cn).

Xu Liu, Chunshui Cao, and Yongzhen Huang are with Watrix Technology Limited Co. Ltd, Beijing 100088, China. (Email: {xu.liu, chunshui.cao}@watrix.ai).

* Equal contributions.

† Project lead.

‡ Corresponding author.

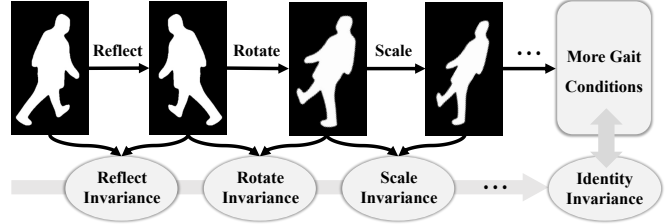


Fig. 1. Different gait conditions are approximately associated with the combination of various geometric transformations, *e.g.*, reflect, rotate, scale. Achieving invariance learning among them is an effective way to achieve identity invariance in gait recognition.

highlighting its practical significance and potential for real-world applications.

In ideal conditions, gait recognition strives to extract *identity-invariant* features of an individual under various conditions. Over a long period, researchers have developed a series of gait datasets [6]–[11] that encompass various gait conditions, including but not limited to normal walking, walking with different clothes, and multiple camera or walking views. Subsequent gait models [12]–[15] aim to extract *common traits* of the same individual across various gait conditions in a data-driven manner for recognition. For example, during training, samples of the same individual across conditions are pulled closer, while those of different individuals are pushed apart. This paradigm has become mainstream and achieved remarkable performance [4], [5], [15]–[19].

However, current gait models largely rely on implicit training with existing *limited* gait conditions. Given the endless variety of conditions present in real-world scenarios, this reliance limits their ability to generalize to unseen conditions. To address this, an alternative strategy is to shift the focus to exploring the broader essence of understanding the explicit relations across different gait conditions. Once this essence is revealed, it becomes possible to establish connections among different gait conditions, thereby making generalization to broader conditions feasible.

As an initial attempt, we propose a new perspective to approximately achieve gait recognition: variations in an individual's gait under different conditions can be approximately viewed as a combination of geometric transformations. For example, as in Fig. 1, (1) A 36-degree gait sequence can approximate a 144-degree sequence by horizontal reflection [8]; (2) A lean-left gait sequence can be approximately generated by rotating an upright posture [6], [10]; (3) The thicker clothing effects can be approximately simulated by scaling [8], [10]. In this way, more complex conditions can be viewed as a combination of geometric transformations. Thus, **achieving**

identity invariance in gait recognition is approximately attainable through geometric invariance.

Based on this new perspective, we focus on two primary questions: (1) Which geometric transformations are most effective for modeling the variations in different gait conditions? (2) How can we achieve invariance across these geometric transformations in gait models?

For the selection of geometric transformations, as an initial attempt, we choose three of the most common geometric transformations, *i.e.*, **Reflect**, **Rotate**, **Scale**. Reflect approximates the changes in reflective walking directions. Rotate simulates the variations in posture, like lean-left or lean-right. Different clothing thicknesses can be considered as a type of Scale. These transformations are prevalent in real-world gait scenarios, and their combination enables handling a wider range of walking conditions. Other geometric transformations are worth further exploration.

To achieve geometric invariance, we propose a *Reflect-Rotate-Scale* invariance learning framework (*RRS-Gait*). The core idea is a two-stage process: it first learns approximately equivariant features, and then aggregates them into invariant features for recognition. For the first equivariance learning stage, it flexibly adjusts its convolution kernels based on the geometric transformation to achieve feature equivariance. For the second invariance learning stage, it introduces a pooling strategy to aggregate these equivariant features into a final invariant representation. Specifically, *RRS-Gait* involves three equivariant modules and a invariant pooling layer: **(1) Reflect Equivariance Learning (ReEL)** module modifies the regular convolutional kernel to include half regular kernels and half *reflected kernels* for feature extraction. The resulting two features are then aggregated along the corresponding channels into reflect-equivariant features. **(2) Adaptive Rotate Equivariance Learning (RoEL)** module predicts rotation angle of each gait sequence and introduces *rotated kernel* design to adapt to rotations for rotate equivariance. **(3) Multi-Scale Equivariance Learning (SEL)** module collects multi-scale features using *various dilated kernels* and designs cross-channel and cross-scale feature interactions to enhance scale equivariance. **(4)** These three kinds of equivariant-aware features are respectively fed into each feature mapping stage with a *pooling* operation to convert equivariant features into invariant ones.

To summarize, the main contributions are as follows:

- We propose a new perspective to achieve gait recognition: the identity invariance under various gait conditions can be approximately achieved by geometric invariance.
- As an initial attempt in this perspective, we explore three common geometric transformations (*i.e.*, Reflect, Rotate, Scale) and their feasible equivariant kernel designs.
- We propose *RRS-Gait*, a *Reflect-Rotate-Scale* invariance learning framework, to achieve geometric equivariance and invariance for given geometric transformations.
- Extensive experiments on Gait3D, GREW, CCPG, and SUSTech1K show superior results across various conditions. For example, *RRS-Gait* achieves 76.7% and 81.0% rank-1 in the challenging Gait3D and GREW.

II. RELATED WORK

A. Gait Recognition

Current gait methods can be primarily divided into two categories: model-based and appearance-based methods. **Model-based methods** [11], [20]–[28] utilize various estimation models to capture human structure (*e.g.*, skeleton, mesh, and point cloud) as input, while **appearance-based methods** [12], [14], [29]–[45] focus on human appearance (*e.g.*, silhouette, parsing and RGB) for recognition. Here we focus on silhouette-based methods, as they are most relevant to our work.

Over a long period, silhouette-based methods often rely on temporal modeling, spatial modeling, or their combined modeling to capture discriminative features. For example, **Spatial modeling** [12], [17], [18], [29]–[31], [38], [46]–[49] involves capturing global structural representations, local fine-grained details, and their interactions. **Temporal modeling** [3], [4], [13], [14], [16], [41], [50]–[54] focuses on inter-frame dynamics, including capturing gait cycles and mining various action sets (*e.g.*, leg lifting, arm swinging), and multi-scale contextual temporal learning. These two strategies have achieved superior performance on in-the-lab gait datasets [8], [9]. When extended to in-the-wild gait datasets [6], [7], to enhance robustness against potential perturbations commonly present in real-world scenarios, recent works [3], [4], [15] have widely adopted additional probabilistic data augmentation (*e.g.*, ~20%, random flipping, random rotation, random erasing) and achieve further improvements. Despite their effectiveness, exploring more intrinsic solutions to establish connections across different gait conditions is of greater importance.

B. Invariance Feature Learning

Invariance feature learning aims to extract features that remain stable under various transformations, making it widely used in computer vision, especially for classification with well-defined category labels [1], [55], [56]. For example, the feature representations of a category under various conditions should be mapped to the same category label. The main strategies to achieve invariance learning include training with data augmentations [57], [58], pooling layers [59], [60], or contrastive learning methods [61], [62].

More recently, invariance feature learning can also be achieved by first implementing equivariance learning, where feature representations change predictably with input transformations, and then aggregating these equivariant features into invariant representations [63]–[66]. Equivariance is crucial for tasks like image segmentation [67] and object detection [68], [69]. For example, the segmentation mask should change in response to transformations of objects in the image, whether they undergo translation, rotation, or other alterations. Equivariance learning often utilizes group theory [70] and has produced milestone works such as group convolutional networks [65], [71], [72] and rotationally equivariant CNNs [63], [64].

III. PRELIMINARIES

A. Why we need Equivariance and Invariance?

We first briefly review some preliminaries of transform-equivariance and transform-invariance [72], [73]. Given an image input \mathcal{X} and a transformation \mathcal{T} , along with the network \mathcal{F} , we can say that:

- \mathcal{F} is equivariant when $\mathcal{F}(\mathcal{T}(\mathcal{X})) = \mathcal{T}(\mathcal{F}(\mathcal{X}))$,
- \mathcal{F} is invariant when $\mathcal{F}(\mathcal{T}(\mathcal{X})) = \mathcal{F}(\mathcal{X})$.

The first property indicates the features extracted by the network \mathcal{F} from input image \mathcal{X} and transformed image $\mathcal{T}(\mathcal{X})$ also satisfy this transformation. As illustrated in Fig. 2, when taking the same image as input (differing only in reflect or not), an equivariant network can extract features consistent with this transformation. However, the regular convolution will produce distinct feature maps. This difference will be more pronounced as the convolution layers deepen, ultimately leading to distinct label predictions for the same image.

The second property indicates the network \mathcal{F} is unaffected by the transformation \mathcal{T} applied to the input. When we obtain the above two equivariant feature maps, a simple spatial global pooling operation can ensure the pooled features are invariant.

For gait recognition, *assuming an individual under different gait conditions as a transformation, feature equivariance enables consistent responses in feature map [73], thereby allowing extracting invariant features through pooling operation [63]–[66] to achieve identity invariance.*

B. How to achieve Equivariance and Invariance?

As illustrated in the right side of Fig. 2, recent studies in equivariant learning [63]–[66] have demonstrated that: *Equivariant features can be achieved by adding extra convolution kernels (share parameters with regular kernel) based on the input transformation, and then aggregate their resulting feature maps along their corresponding channels into a compact representation.* Through explicitly integrating geometric transformation priors into kernel design, the model naturally ensures the produced features are in a predictable manner, *i.e.*, equivariance. For example, Fig. 2 shows that the reflection transformation equivariance can be achieved by introducing the reflected convolution kernel. Additionally, some other works [74], [75] also explore *flexibly adjusting the convolution*

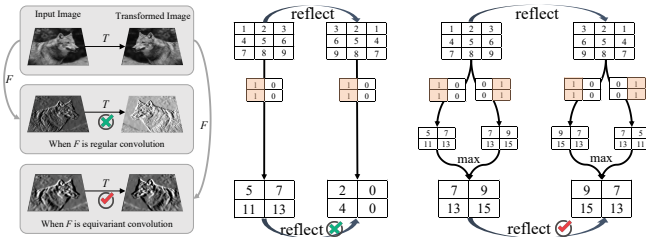


Fig. 2. An example [66] illustrates equivariance in convolution. When applying a reflection transformation to the input image, the regular convolution kernel will produce non-equivariant feature maps, *i.e.*, $\mathcal{F}(\mathcal{T}(\mathcal{X})) \neq \mathcal{T}(\mathcal{F}(\mathcal{X}))$. However, by introducing *both regular kernel and its reflect kernel* for feature extraction, and applying max operation along their corresponding channels, we can obtain equivariant feature maps, *i.e.*, $\mathcal{F}(\mathcal{T}(\mathcal{X})) = \mathcal{T}(\mathcal{F}(\mathcal{X}))$.

kernel based on the input transformation can achieve approximate equivariance. Finally, the equivariant features can be simply pooled into a vector to achieve invariance.

IV. PROPOSED METHOD

In this paper, we select three geometric transformations (*i.e.*, Reflect, Rotate, Scale) as an initial attempt to simulate different gait conditions. Subsequently, as in Fig. 3, **R&S-Gait** proposes three equivariance learning modules and corresponding pooling layers for final invariance feature learning.

A. ReEL: Reflect Equivariance Learning

* **Necessity.** Various walking directions of an individual make gait sequences involving multiple walking views. To improve feature consistency issues among them, researchers often construct rich cross-view conditions within in-the-lab settings [8], [9]. When shifting to in-the-wild settings, the uncontrolled and limited camera views will bring another sparse-view issue [6], [7], [76]. Based on this, Reflect Equivariance Learning (ReEL) is beneficial and necessary to address the above issues from two aspects:

- For in-the-lab case, ReEL helps bring closer the gait sequences from reflectively related views.
- For in-the-wild case, ReEL helps the gait model adapt to the absent reflective view.

* **Solution.** As shown in the left part of Fig. 3, we modify the regular convolution kernel to include *half regular kernels* and *half reflected kernels* for feature extraction. Note that kernel reflection is not equal to feature map reflection. Like the Sobel kernel design in edge detection [77], [78], the horizontal kernel and vertical kernel capture different features, *i.e.*, horizontal edges and vertical edges. Then the extracted features with regular and reflected kernels will be aggregated along the corresponding channels (named Group Pool) to obtain a reflect-equivariant feature. In this case, as shown in Fig. 2, whether the input is the original image or the reflected image, they will ultimately be aggregated into this unified feature to achieve reflect equivariance.

B. RoEL: Adaptive Rotate Equivariance Learning

* **Necessity.** Considering both indoor and outdoor gait data are usually collected from monitoring or other uncontrolled scenarios, different camera angles will cause various left or right rotation in different gait sequences [6], [7]. However,

- Regular CNNs primarily focus on translation invariance but struggle with rotation variances [68], [79], [80].
- Researchers [15] often use probabilistic ($\sim 20\%$) rotate augmentation with a small range of angle (*e.g.*, $\pm 10^\circ$) to adapt to rotated samples, but this *pre-defined* strategy relies on the empirical setting. A large probability or angle may degrade the performance [10], [15].

Thus, it is necessary to *adaptively mitigate rotation variances*, while *covering a broader range of samples*.

* **Difficulty.** If following reflect kernel design in Sec. IV-A, adding *rotate-equivariant* kernels seems straightforward. However, this is not efficient from two aspects:

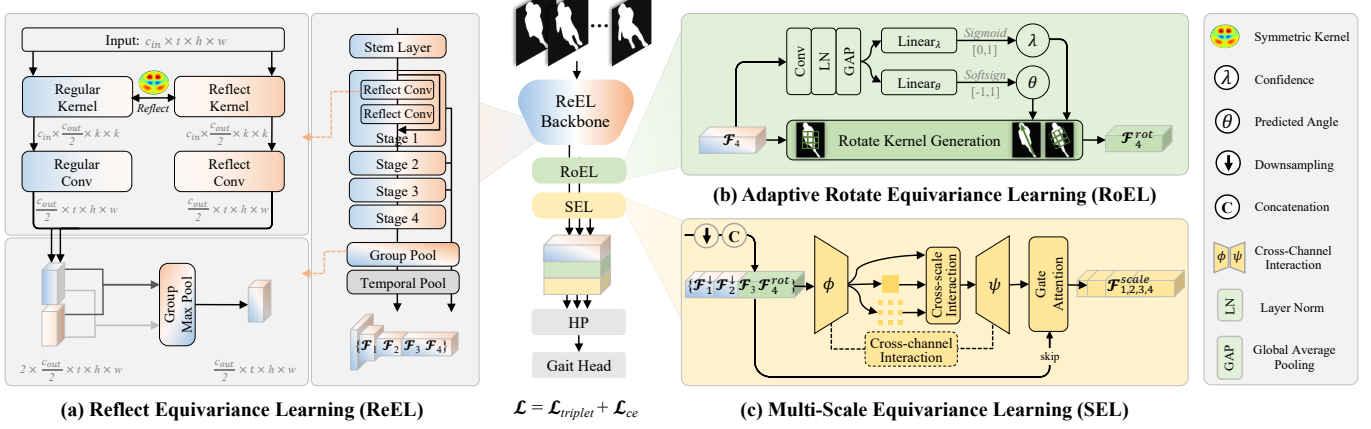


Fig. 3. *Reflect-Rotate-Scale* invariance learning framework (*RRS-Gait*) involves three equivariance learning modules and corresponding invariant pooling layers: (a) Reflect Equivariance Learning (ReEL) module, (b) Adaptive Rotate Equivariance Learning (RoEL) module, and (c) Multi-Scale Equivariance Learning (SEL) module respectively introduce *reflect* kernels, *rotate* kernels, and *multiple dilated* kernels to achieve feature equivariance or approximate equivariance. These equivariant features are then fed into corresponding Horizontal Pooling (HP) layers with a global pooling operation to achieve final feature invariance or approximate invariance.

- **About equivariance.** Unlike reflection that has fixed and limited $\{2\}$ transformations (*i.e.*, reflect or not), rotation is continuous and infinite $\{0^\circ\text{--}360^\circ\}$. Only by involving all angles to conduct rotated kernels can we achieve the strict equivariance learning. However, in practice, we can only choose discrete sampling angles, which will lead to approximate equivariance.
- **About efficiency.** Although approximate equivariance may also be acceptable, each rotated angle requires doubling the number of kernels, exponentially increasing computational cost. However, infinitely halving kernels like Sec. IV-A to maintain efficiency is not feasible.

* **Solution.** As shown in Fig. 3(b), to search for a trade-off between effectiveness and efficiency, motivated by recent advancements in convolutional research [75], [81], we introduce **Adaptive Rotate Equivariance Learning (RoEL)** to adaptively predict the rotated angle of each gait sequence in a data-driven manner, and then adaptively perform rotate convolution for approximate rotate equivariance. All involve the following five steps:

Step 1: Feature Selection. Accurate prediction of gait rotated angle requires reliable features. We empirically select last-stage features ($\mathcal{F}'_4 \in \mathbb{R}^{C_4 \times T \times \frac{H}{4} \times \frac{W}{4}}$) for this purpose.

Step 2: Temporal Aggregation. Since gait sequence is often captured by the same camera in a short time, they largely share a similar rotated angle. Thus, we introduce *Temporal Max Pooling* to aggregate the maximum response of temporal features, which is also suitable for mitigating the impact of abnormal or redundant frames and reducing calculations.

$$\mathcal{F}_4 = \text{TemporalAgg}(\mathcal{F}'_4), \mathcal{F}_4 \in \mathbb{R}^{C_4 \times \frac{H}{4} \times \frac{W}{4}}. \quad (1)$$

Step 3: Rotated Angle Prediction (θ) and Confidence (λ). As in Fig. 3, the output feature ($\mathcal{F}_4 \in \mathbb{R}^{C_4 \times \frac{H}{4} \times \frac{W}{4}}$) is first processed by a convolution, layer normalization, and ReLU activation to effectively extract spatial features and ensure feature stability. Then, this feature undergoes Global Average Pooling

(GAP) to eliminate spatial dimensions ($\mathbb{R}^{C_4 \times 1}$). Finally, it will be fed into two *independent* branches to simultaneously learn the rotated angle (θ) and confidence (λ). Each branch includes a linear layer ($C_4 \rightarrow 1$) and an activation function. The difference between them is the selection of activation function: the rotated angle can be positive or negative, so it uses Softsign [82] to output in the range $[-1, 1]$, while the confidence branch uses Sigmoid [83] to output in the range $[0, 1]$. Additionally, the angle will not be multiplied by 360° but by a limited angle (*e.g.*, $\theta_{limit} = 20^\circ/30^\circ/40^\circ/50^\circ$) since human body usually leans within a limited range. The overall are as follows:

$$\mathcal{F}_{init}^{rot} = \text{GAP}(\text{ReLU}(\text{LayerNorm}(\text{Conv2d}(\mathcal{F}_4))), \quad (2)$$

$$\theta = \text{Softsign}(\text{Linear}_\theta(\mathcal{F}_{init}^{rot})) \cdot \theta_{limit}, \theta \in \mathbb{R}^1, \quad (3)$$

$$\lambda = \text{Sigmoid}(\text{Linear}_\lambda(\mathcal{F}_{init}^{rot})), \lambda \in \mathbb{R}^1. \quad (4)$$

Step 4: Adaptive Rotated Kernel Generation ($\mathcal{K} \rightarrow \mathcal{K}_\theta$). Based on the regular kernel (\mathcal{K}) and the predicted angle (θ), we construct the adaptive rotation matrix and utilize bilinear interpolation to generate the final rotated kernel (\mathcal{K}_θ).

$$\mathcal{K}_\theta = \text{Rotate}(\mathcal{K}, \theta), \{\mathcal{K}, \mathcal{K}_\theta\} \in \mathbb{R}^{C_4 \times C_4 \times k \times k}, \quad (5)$$

where C_4 and k are input/output channels and kernel size.

Step 5: Adaptive Rotate Convolution. The generated rotated kernel (\mathcal{K}_θ) replaces regular kernel (\mathcal{K}) for adaptive rotation convolution with confidence (λ) as follows:

$$\mathcal{F}_4^{rot} = \lambda \cdot \mathcal{K}_\theta(\mathcal{F}_4), \{\mathcal{F}_4^{rot}, \mathcal{F}_4\} \in \mathbb{R}^{C_4 \times \frac{H}{4} \times \frac{W}{4}}. \quad (6)$$

C. SEL: Multi-Scale Equivariance Learning

* **Necessity.** Similar to Reflect and Rotate, the Scale variance is also common in gait field. Wearing a coat or skirt will cause scale variations in the shape of human body. This inspires researchers to construct corresponding gait conditions (*e.g.*, cloth-changing [10]) to simulate scale variance, but it remains highly challenging and has not achieved satisfactory results.

* **Difficulty.** Similar to Rotate, Scale transformations are also continuous and infinite $\{\infty\}$. How to adaptively adapt to various scale variations while maintaining efficiency is just as urgent as addressing Rotate variances.

* **Solution.** To simulate scale transformations and mitigate scale variances, we introduce **Multi-Scale Equivariance Learning (SEL)**. It collects multi-scale features in each layer as the initial input and designs *multiple dilated kernels* to further simulate scale variances, facilitating the following multi-scale interactions to mitigate scale variance and achieve approximate scale equivariance, involving:

Step 1: Multi-scale Feature Selection. To obtain multi-scale gait representations, we select the output of each layer in backbone $(\mathcal{F}_1, \mathcal{F}_2, \mathcal{F}_3, \mathcal{F}_4^{rot})$, as they involve varying spatial resolutions and receptive fields due to subsampling layers and convolutions of different depths in the backbone.

Step 2: Feature Initialization. To ensure efficiency, we assume scale variances of frames within a gait sequence are similar since they are always captured by the same camera in a short time. We adopt *Temporal Max Pooling* as Eq. (1) to aggregate the maximum response of temporal features. Then, all of them are downsampled to the same resolution $(\mathbb{R}^{C_i \times \frac{H}{4} \times \frac{W}{4}})$ based on bilinear interpolation and concatenated along channel dimension to obtain initial scale-orient feature $(\mathcal{F}_{init}^{scale} \in \mathbb{R}^{(C_1+C_2+C_3+C_4) \times \frac{H}{4} \times \frac{W}{4}})$ as follows.

$$\mathcal{F}_{init}^{scale} = \underset{C}{\text{Concat}}(\mathcal{F}_1^{\downarrow}, \mathcal{F}_2^{\downarrow}, \mathcal{F}_3, \mathcal{F}_4^{rot}). \quad (7)$$

Step 3: Cross-Channel Interaction Module. Based on the initial scale-orient features $(\mathcal{F}_{init}^{scale})$, we simply introduce a convolution layer with batch normalization and a nonlinear layer to implement channel reduction, facilitating cross-channel interaction to mix multi-scale features.

$$\phi: \mathcal{F}_c^{scale} = \text{ReLU}(\text{BN}(\text{Conv2d}(\mathcal{F}_{init}^{scale}))). \quad (8)$$

Step 4: Cross-Scale Interaction Module. To better capture multiple scales for spatial interaction, we further introduce multi-scale convolutions based on: (s1) no operation as the original feature, (s2) kernel=3, and (s3) kernel=5, to obtain three spatial scales, *i.e.*, $\mathcal{F}_{s_1}^{scale}$, $\mathcal{F}_{s_2}^{scale}$, and $\mathcal{F}_{s_3}^{scale}$.

Subsequently, we flatten the spatial dimension of these three scales and apply vanilla self-attention [84] for multi-scale interaction. Specifically, the original feature (s1) serve as the query and the other two (s2, s3) are regarded as key and value to achieve cross-scale attention, followed by the vanilla Feed Forward (FFN) layer [84].

$$q = W_q \cdot \mathcal{F}_{s_1}^{scale}, k = W_k \cdot \mathcal{F}_{s_2}^{scale}, v = W_v \cdot \mathcal{F}_{s_3}^{scale}, \mathcal{F}_s^{scale} = \text{FFN}(\text{Softmax}(\frac{q \cdot k^T}{\sqrt{C/r}}) \cdot v), \quad (9)$$

where W_q , W_k , and W_v are weights of linear layer as [84].

Step 5: Gate Attention. Finally, we introduce gate attention with residual connection to mitigate early training instability and improve optimization. Specifically, we first expand the channels of \mathcal{F}_s^{scale} to the original size ($C/r \rightarrow C$), which can be viewed as a second cross-channel interaction.

$$\psi: \mathcal{F}_s^{scale} \leftarrow \text{ReLU}(\text{BN}(\text{Conv2d}(\mathcal{F}_s^{scale}))), \quad (10)$$

Then, it will be split into four outputs with the same size of $\mathcal{F}_i \in \{\mathcal{F}_1^{\downarrow}, \mathcal{F}_2^{\downarrow}, \mathcal{F}_3, \mathcal{F}_4^{rot}\}$ along the channel dimension. The overall gate attention is as follows:

$$\mathcal{F}_i^{scale} = \text{Sigmoid}(\text{BN}(\text{Conv2d}_i(\mathcal{F}_{s,i}^{scale}))) \cdot \mathcal{F}_{s,i}^{scale} + \mathcal{F}_i, \quad (11)$$

where \mathcal{F}_i^{scale} indicates the scaled features, $i = 1, 2, 3, 4$.

D. Invariant Representation and Loss Function

Invariant Representation. To this end, we obtain three equivariant or approximately equivariant features: Reflect (\mathcal{F}_4), Rotate (\mathcal{F}_4^{rot}), and Scale ($\mathcal{F}_{1,2,3,4}^{scale}$). Following recent works [18], [30], [31], as in Table II, each of them will be horizontally partitioned into P parts, followed by Horizontal Pooling (HP) [12], Separate Fully Connected layers [12], and BNNeck [12] as Gait Head for final feature learning. Notably, *the spatial global pooling of each part in HP converts equivariant features into the vectors, supporting our final invariance learning*.

Loss Function. The loss function follows the current popular gait method [3] and uses triplet and cross-entropy loss.

V. EXPERIMENTS

A. Datasets and Implementation Details

Datasets. We select four of the most recent and challenging gait datasets for evaluation, involving both outdoor and indoor settings, *i.e.*, Gait3D [6], GREW [7], CCPG [10], and SUSTech1K [11]. The details are shown in Table I. We strictly adhere to the established protocols of these datasets, and all data pertaining to human subjects comply with ethical and privacy review requirements.

Implementation Details. (1) During data pretreatment, all silhouettes are normalized to 64×44 resolution. (2) During training, we strictly follow the official dataset settings [6], [7], [10], [11] and popular training strategies from recent gait project (OpenGait [3], [15]). These include a (P, K) sampling strategy in a mini-batch (sampling P identities with K gait sequences per identity, and each sequence consists of a fixed 30 frames), as well as the optimizer, milestones, and total steps. (3) During test, all frames in a gait sequence are sent to the model for evaluation with Euclidean distance similarity. (4) For model design, the number of layers $[l_1, l_2, l_3, l_4]$ in \mathcal{RRS} -Gait-S are set to $[1, 1, 1, 1]$ for CCPG and SUSTech1K as they are collected from controlled environments, while in \mathcal{RRS} -Gait-L are set to $[1, 4, 4, 1]$ for Gait3D and $[2, 4, 4, 2]$ for GREW to suit uncontrolled collections and large-scale datasets. The ReflectConv in Table II is set to 2D-Conv-based [15] in CCPG and SUSTech1K, and P3D-Conv-based [3] in Gait3D and GREW. Our baseline also follows these settings for a fair comparison, named Baseline-S and Baseline-L. The part number in Horizontal Pooling of each feature is set to $P=16$. The angle limit in Eq. (3) is set as $\theta_{limit}=40^\circ$. The channel reduction r in Eq. (8,10) is 4. The weight β in the loss function is set to 1.0. The margin in triplet loss is set to 0.2. (5) For other details, the parameters and FLOPs are based on the Backbone for consistency across different datasets, as they have varying numbers of classifications that can lead to

TABLE I

IMPLEMENTATION DETAILS ON BOTH INDOOR AND OUTDOOR DATASETS. #IDs AND #SEQS INDICATE THE TOTAL SUBJECTS AND SEQUENCES. #LR AND #WD ARE THE INITIAL LEARNING RATE AND WEIGHT DECAY FOR THE OPTIMIZER.

Environments	Datasets	Train Phase		Test Phase		Batch (P, K)	Optimizer	Milestones		Total Iters
		#IDs	#Seqs	#IDs	#Seqs			(20K,40K,50K)	(80K,120K,150K)	
Outdoor	Gait3D [6]	3,000	18,940	1,000	6,369	(32, 4)	SGD	(20K,40K,50K)	(80K,120K,150K)	60K
	GREW [7]	20,000	102,887	6,000	24,000	(32, 4)	#lr=0.1	(20K,30K)	(20K,30K)	180K
	SUSTech1K [11]	250	6,011	800	19,228	(8, 8)	#wd=0.0005	(20K,30K)	(20K,30K)	40K
Indoor & Outdoor	CCPG [10]	100	8,187	100	8,095	(8, 16)	momentum=0.9	(20K,40K,50K)	(20K,40K,50K)	60K

TABLE II

ARCHITECTURE OF \mathcal{RRS} -GAIT. ReflectConv INDICATES REFLECT CONVOLUTION TO REPLACE REGULAR CONVOLUTION. “T”, “C” DENOTE SEQUENCE LENGTH AND OUTPUT CHANNELS. STRIDE AND RESIDUAL ARE OMITTED FOR SIMPLICITY. $C=32 \times 2$ MEANS 32 CHANNELS ARE FROM REGULAR KERNELS AND ANOTHER 32 FROM REFLECTED KERNELS. “ l_i ” IS THE NUMBER OF LAYERS IN EACH STAGE. THE COLOR HIGHLIGHTS OUR MODIFICATIONS.

Layer	Output	\mathcal{RRS} -Gait
Stem	$T \times H \times W$	ReflectConv2D, Kernel = 3, $C = 32 \times 2$
Stage 1	$T \times H \times W$	$\left[\begin{array}{l} \text{ReflectConv2D, Kernel = 3, } C = 32 \times 2 \\ \text{ReflectConv2D, Kernel = 3, } C = 32 \times 2 \end{array} \right] \times l_1$
Stage 2	$T \times \frac{H}{2} \times \frac{W}{2}$	$\left[\begin{array}{l} \text{ReflectConv, Kernel = 3, } C = 64 \times 2 \\ \text{ReflectConv, Kernel = 3, } C = 64 \times 2 \end{array} \right] \times l_2$
Stage 3	$T \times \frac{H}{4} \times \frac{W}{4}$	$\left[\begin{array}{l} \text{ReflectConv, Kernel = 3, } C = 128 \times 2 \\ \text{ReflectConv, Kernel = 3, } C = 128 \times 2 \end{array} \right] \times l_3$
Stage 4	$T \times \frac{H}{4} \times \frac{W}{4}$	$\left[\begin{array}{l} \text{ReflectConv, Kernel = 3, } C = 256 \times 2 \\ \text{ReflectConv, Kernel = 3, } C = 256 \times 2 \end{array} \right] \times l_4$
GPool	$T \times \frac{H}{4} \times \frac{W}{4}$	Group Pool ($C = 256 \times 2 \rightarrow 256$)
TP	$1 \times \frac{H}{4} \times \frac{W}{4}$	Temporal Max Pooling ($T \rightarrow 1$)
RoEL	$1 \times \frac{H}{4} \times \frac{W}{4}$	Adaptive Rotate Equivariance Learning
SEL	$1 \times \frac{H}{4} \times \frac{W}{4}$	Multi-Scale Equivariance Learning
HP	$1 \times 3P$	Horizontal Pooling [12]
Head	$1 \times 3P$	Separate Fully Connected Layers & BNNeck [12]

different results. All results are based on NVIDIA RTX 3090 with PyTorch 2.2.

B. Comparisons with State-of-the-Art

Comparisons in CCPG and SUSTech1K. As shown in Table IV and Table V, \mathcal{RRS} -Gait achieves consistent improvement. Notably, the data collection settings for CCPG include more diverse scale transformations due to clothing changes and variations in body rotation (left or right) in surveillance camera views. SUSTech1K incorporates different camera distances, multiple views, and other various settings. Despite these challenges, \mathcal{RRS} -Gait achieves substantial performance gains, with an average rank-1 improvement of +6.1% on CCPG and +4.3% on SUSTech1K.

Comparisons in Gait3D and GREW. As shown in Table III, \mathcal{RRS} -Gait achieves superior performance compared to existing gait models on the challenging Gait3D and GREW. The performance gains stem from the selected three transformations, which frequently appear in real-world scenarios

TABLE III

SINGLE-DOMAIN EVALUATION RESULTS ON GAIT3D [6] AND GREW [7] DATASETS WITH RANK, MAP, AND MINP ACCURACY (%). THE **BOLD** INDICATES BEST RESULT.

Method	Venue	Gait3D [6]			GREW [7]	
		R-1	R-5	mAP	R-1	R-5
GaitGraph2 [23]	CVPRW'22	11.2	-	-	34.8	-
GaitTR [85]	ES'23	7.2	-	-	48.6	-
PAA [22]	ICCV'23	38.9	-	-	38.7	62.1
SkeletonGait [21]	AAAI'24	38.1	56.7	28.9	77.4	87.9
GaitSet [12]	AAAI'19	36.7	58.3	30.0	46.3	63.6
GaitPart [13]	CVPR'20	28.2	47.6	21.6	44.0	60.7
GaitGL [14]	ICCV'21	29.7	48.5	22.3	47.3	63.6
CSTL [50]	ICCV'21	11.7	19.2	5.6	50.6	65.9
DANet [51]	CVPR'23	48.0	69.7	-	-	-
GaitGCI [17]	CVPR'23	50.3	68.5	39.5	68.5	80.8
GaitBase [15]	CVPR'23	64.6	-	55.2	60.1	-
HSTL [18]	ICCV'23	61.3	76.3	55.5	62.7	76.6
DyGait [16]	ICCV'23	66.3	80.8	56.4	71.4	83.2
GaitSSB [86]	TPAMI'23	63.6	-	-	61.7	-
CLASH [87]	TIP'24	52.4	69.2	40.2	67.0	78.9
HiH-S [35]	ArXiv'23	72.4	86.9	64.4	72.5	83.6
QAGait [34]	AAAI'24	67.0	81.5	56.5	59.1	74.0
DeepGaitV2 [3]	ArXiv'23	74.4	88.0	65.8	77.7	88.9
VPNet-L [4]	CVPR'24	75.4	87.1	-	80.0	89.4
CLTD [19]	ECCV'24	69.7	85.2	-	78.0	87.8
FreeLunch [36]	ECCV'24	70.1	-	61.9	65.5	78.7
GaitMoE [5]	ECCV'24	73.7	-	66.2	79.6	89.1
Baseline-L (Ours)		74.4	88.0	65.8	79.2	89.2
\mathcal{RRS}-Gait-L (Ours)		76.7	89.9	69.6	81.0	89.9

and often mislead model predictions. Our \mathcal{RRS} -Gait demonstrates higher mAP performance compared to rank-1 (+3.8% vs. +2.3% in Gait3D), underscoring its better stability, with a more promising improvement in mAP than rank-1 on Gait3D (+4.4% vs. +3.3%).

C. Ablation Study

If not specific, we utilize CCPG and Gait3D to conduct ablation studies. The CCPG results are based on the gait protocol, excluding the identical-views cases. The Reflect, Rotate, and Scale are short for our designed Reflect Invariance Learning (ReEL), Adaptive Rotate Invariance Learning (RoEL), and Multi-Scale Invariance Learning (SEL) modules.

Ablation of ReEL, RoEL, SEL. As in Table VI, we can observe that the ReEL, RoEL, and SEL modules can progressively improve performance, *i.e.*, they achieve +4.5%, +0.4%,

TABLE IV

COMPARISON RESULTS ON CCPG [10] DATASET BASED ON GAIT AND ReID EVALUATION PROTOCOLS WITH RANK-1 ACCURACY (%). THE **BOLD** INDICATES BEST RESULT.

Method	Venue	Gait Evaluation Protocol (R-1)					ReID Evaluation Protocol (R-1)				
		CL	UP	DN	BG	Mean	CL	UP	DN	BG	Mean
GaitGraph2 [23]	CVPRW'22	5.0	5.3	5.8	6.2	5.6	5.0	5.7	7.3	8.8	6.7
GaitTR [85]	ES'23	15.7	18.3	18.5	17.5	17.5	24.3	28.7	31.1	28.1	28.1
SkeletonGait [21]	AAAI'24	40.4	48.5	53.0	61.7	50.9	52.4	65.4	72.8	80.9	67.9
GaitSet [12]	AAAI'19	60.2	65.2	65.1	68.5	64.8	77.5	85.0	82.9	87.5	83.2
GaitPart [13]	CVPR'20	64.3	67.8	68.6	71.7	68.1	79.2	85.3	86.5	88.0	84.8
AUG-OGBase [10]	CVPR'23	52.1	57.3	60.1	63.3	58.2	70.2	76.9	80.4	83.4	77.7
GaitBase [15]	CVPR'23	71.6	75.0	76.8	78.6	75.5	88.5	92.7	93.4	93.2	92.0
Baseline-S (Ours)		71.8	75.8	77.1	79.0	75.9	88.5	92.9	93.0	93.2	91.9
$\mathcal{R}\mathcal{R}\mathcal{S}$ -Gait-S (Ours)		78.4	81.8	81.9	85.7	82.0	91.8	96.5	94.4	96.2	94.7

TABLE V

COMPARISON RESULTS ON SUSTECH1K [11] DATASET WITH VARIOUS CONDITIONS UNDER RANK-1 AND RANK-5 ACCURACY (%). THE **BOLD** INDICATES BEST RESULT.

Method	Venue	Probe Sequence (R-1)								Overall	
		Normal	Bag	Clothing	Carrying	Umberalla	Uniform	Occlusion	Night	R-1	R-5
GaitGraph2 [23]	CVPRW'22	22.2	18.2	6.8	18.6	13.4	19.2	27.3	16.4	18.6	40.5
GaitTR [85]	ES'23	33.3	31.5	21.0	30.4	22.7	34.6	44.9	23.5	30.8	56.0
SkeletonGait [21]	AAAI'24	67.9	63.5	36.5	61.6	58.1	67.2	79.1	50.1	63.0	83.5
GaitSet [12]	AAAI'19	69.1	68.2	37.4	65.0	63.1	61.0	67.2	23.0	65.0	84.8
GaitPart [13]	CVPR'20	62.2	62.8	33.1	59.5	57.2	54.8	57.2	21.7	59.2	80.8
GaitGL [14]	ICCV'21	67.1	66.2	35.9	63.3	61.6	58.1	66.6	17.9	63.1	82.8
GaitBase [15]	CVPR'23	81.5	77.5	49.6	75.8	75.5	76.7	81.4	25.9	76.1	89.4
Baseline-S (Ours)		81.5	77.8	49.7	75.6	75.3	75.9	81.8	25.9	76.0	89.5
$\mathcal{R}\mathcal{R}\mathcal{S}$ -Gait-S (Ours)		85.7	82.2	52.3	79.7	81.4	81.0	87.3	29.0	80.3	92.0

TABLE VI

ABLATIONS OF $\mathcal{R}\mathcal{R}\mathcal{S}$ -GAIT. THE **BOLD** INDICATES BEST RESULT.

Conditions	CCPG (Gait)				Gait3D	
	CL	UP	DN	BG	R-1	mAP
$\mathcal{R}\mathcal{R}\mathcal{S}$ -Gait (Ours)	78.4	81.8	81.9	85.7	76.7	69.6
1. Ablation of each component						
w/o SEL	77.2	81.3	81.6	84.6	75.9	67.8
w/o SEL, RoEL	76.8	80.2	81.3	82.8	-	-
w/o SEL, RoEL, ReEL	72.3	76.1	76.9	78.9	73.4	65.2
2. Ablation of angle limit (θ_{limit}) in RoEL						
w/ $\theta_{limit} = 50^\circ$	77.3	81.3	81.5	84.3	75.8	67.6
w/ $\theta_{limit} = 40^\circ$	77.2	81.3	81.6	84.6	75.9	67.8
w/ $\theta_{limit} = 30^\circ$	75.6	78.3	78.1	82.2	75.4	67.1
w/ $\theta_{limit} = 20^\circ$	75.6	78.4	78.8	81.5	74.8	66.3
3. Ablation of each component in SEL						
w/ Stage 1-2-3-4	78.4	81.8	81.9	85.7	76.7	69.6
w/ Stage 2-3-4	77.1	81.2	80.7	85.4	76.1	68.5
w/o Cross-Channel Interaction	77.8	81.4	81.7	85.6	76.0	69.2
w/o Cross-Scale Interaction	77.6	81.5	81.4	85.4	74.6	67.1
w/o Gate Attention	77.8	81.7	81.8	85.2	76.2	69.2

+1.2% rank-1 accuracy in the challenging CL condition in CCPG. Meanwhile, the RoEL and SEL modules also achieve +2.6% and +1.8% mAP in Gait3D.

Ablation of Group Pool in ReEL module. GPool is crucial to ensure reflect equivariance. Although its necessity is theoretically guaranteed, we also conduct the ablation study

TABLE VII

ABLATION OF GPOOL IN Reflect MODULE. C=32 \times 2 MEANS 32 CHANNELS ARE FROM REGULAR KERNELS AND ANOTHER 32 ARE FROM REFLECTED KERNELS. GPool AGGREGATES REGULAR AND REFLECTED FEATURES ALONG CHANNELS BEFORE FEEDING THEM INTO THE FULLY CONNECTED LAYER. THE **BOLD** INDICATES BEST RESULT.

Condition	Backbone		CCPG (R-1)			
	#Last Channels	#FC Layer	CL	UP	DN	BG
Baseline	C=512	512 \rightarrow 256	72.3	76.1	76.9	78.9
w/o GPool	C=256 \times 2 = 512	512 \rightarrow 256	75.8	78.5	79.7	83.4
w/ GPool	C=256 \times 2 \rightarrow 256	256 \rightarrow 256	76.8	80.2	81.3	82.8

on GPool. Table VII shows that model performance drops by -1.0% (CCPG-CL) without GPool but remains +3.5% higher than the baseline. This confirms the theoretical necessity and practical importance of GPool in the ReEL module.

Ablation of rotate limit (θ_{limit}) in RoEL module. Due to the distinctive upright walking pattern of humans, the deviation angles to the left or right are always small. Even under abnormal surveillance angles, the deviation remains limited (*i.e.*, the angle between human body and vertical axis in an image is limited). We define this angle limit as a hyper-parameter and ablation results in Table VI show that 40° limit is effective, with larger values (*e.g.* $\geq 50^\circ$) providing no additional benefit as performance stabilizes.

Ablation of SEL module. To achieve effective multi-scale interaction, we design three sub-modules: Selecting features from various layers with different spatial scales, cross-channel

TABLE VIII

COMPARISONS WITH BACKBONE PARAMETERS (M) AND FLOPs (G). THE RESULTS ARE BASED ON 30 FRAMES WITH 64×44 RESOLUTION. THE **BOLD** INDICATES THE BEST RESULT.

Condition	Backbone		CCPG (R-1)				
	#Paras.	#FLOPs	CL	UP	DN	BG	
Baseline	4.90M	35.490G	72.3	76.1	76.9	78.9	
w/ ReIL	1.66M	35.490G	76.8	80.2	81.3	82.8	
w/ ReIL, RoIL	2.25M	35.491G	77.2	81.3	81.6	84.6	
w/ ReIL, RoIL, SIL	3.56M	36.074G	78.4	81.8	81.9	85.7	

TABLE IX

CROSS-DOMAIN EVALUATIONS UNDER RANK-1 ACCURACY. THE **BOLD** INDICATES THE BEST RESULT.

Source Dataset	Method	Target Dataset			
		CCPG (Gait-CL)	SUSTech1K (Overall)	Gait3D (Rank-1)	GREW (Rank-1)
CCPG	Baseline	72.3	17.4	13.0	13.2
	RRS-Gait	78.4	26.7	19.2	16.7
SUSTech1K	Baseline	16.3	76.0	12.9	12.2
	RRS-Gait	20.4	80.3	20.9	15.7
Gait3D	Baseline	13.4	50.2	73.4	35.5
	RRS-Gait	15.5	50.5	76.7	36.9
GREW	Baseline	12.2	29.1	32.6	79.2
	RRS-Gait	13.3	29.4	34.6	81.0

and cross-scale interactions to adapt to different scales, and gate attention to maintain training stability. Ablation results in Table VI show that: (1) Select layers 1-2-3-4 is more effective than layers 2-3-4 (69.6% vs. 68.5% mAP on Gait3D); (2) Both cross-channel and cross-scale interactions provide better performances, with cross-scale interactions yielding greater gains; (3) Gate attention also proves effective on both datasets.

Visualization of each module. Fig. 4 shows that: (1) The ReEL module can flexibly adapt to each frame and achieve a periodic-like response by focusing on specific actions at particular moments. (2) The output of RoEL module shows a clear lean-right response due to the application of rotated convolution with the predicted angle. (3) The SEL module captures more fine-grained and key-region responses to form a more detailed representation.

D. Discussion

Discussion about Computational Cost As stated in the manuscript, we halve the number of kernels in ReIL module to maintain efficiency. Table VIII shows that this modification can maintain the FLOPs (35.490G remains 35.490G), reduce parameters ($4.90M \rightarrow 1.66M$), but still achieve high performance ($72.3\% \rightarrow 76.8\%$, CCPG-CL). Additionally, the input features undergo Temporal Max Pooling to reduce the temporal dimension in RoIL and SIL modules. Even with an increase in parameters (0.59M and 1.31M), computational efficiency is maintained, with only a minimal increase in FLOPs (0.001G and 0.583G).

More Results about Cross-domain Evaluation As shown in Table IX, compared to our baseline, *RRS-Gait* also achieves

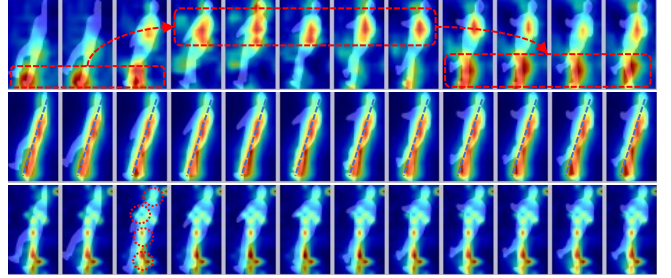


Fig. 4. Visualizations of ReEL, RoEL, and SEL outputs (from up to bottom). RoEL or SEL shares the same heatmap across frames since their features undergo temporal pooling.

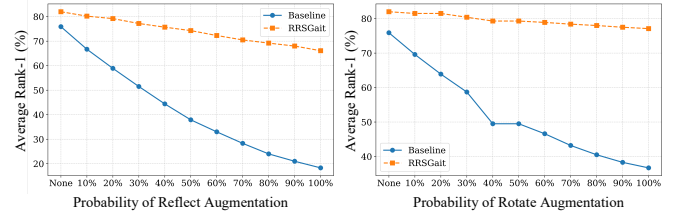


Fig. 5. Geometric invariance evaluations through applying varying probabilities of data augmentation (*i.e.*, random reflection and rotation) during the test stage on CCPG.

better generalization results across all four gait datasets. These results further validate the applicability of our model under a broader range of gait conditions.

More results about geometric invariance. As in Fig. 5, to verify our *RRS-Gait* can effectively mitigate the geometric transformations, we introduce varying levels (*i.e.*, probabilities) of data augmentation (*i.e.*, random reflection or rotation) during the test stage. The results show that *RRS-Gait* remains stable, with only a slight drop in performance. We omit scale augmentation due to the current gait field lacking a standard scale augmentation, leaving it for further exploration.

Limitations. (1) As an initial attempt to leverage geometric invariance to achieve identity invariance, we select three common geometric transformations. More geometric transformations are worth further research to better develop this approach. (2) We design distinct equivariant kernels to suit the proposed geometric transformations. It is worthwhile to explore a universal kernel design or aggregate these equivariant kernels into a compact kernel like structural re-parameterizing [88].

VI. CONCLUSION

In this paper, we propose a new perspective: different gait conditions can be approximately linked through geometric transformations, thereby enabling identity invariance in gait recognition via geometric invariance. As an initial attempt, we explore three geometric transformations (*i.e.*, reflect, rotate, and scale), and propose a Reflect-Rotate-Scale invariance learning framework, named *RRS-Gait*. Extensive experiments and visualizations show consistent improvements in both indoor and outdoor gait datasets. We hope this new perspective will inspire further exploration of more geometric transformations to connect different gait conditions for better gait recognition.

REFERENCES

[1] C. Shen, S. Yu, J. Wang, G. Q. Huang, and L. Wang, “A comprehensive survey on deep gait recognition: Algorithms, datasets and challenges,” *arXiv preprint arXiv:2206.13732*, 2022.

[2] V. Rani and M. Kumar, “Human gait recognition: A systematic review,” *Multimedia Tools and Applications*, pp. 1–35, 2023.

[3] C. Fan, S. Hou, J. Liang, C. Shen, J. Ma, D. Jin, Y. Huang, and S. Yu, “Opengait: A comprehensive benchmark study for gait recognition towards better practicality,” *IEEE Transactions on Pattern Analysis and Machine Intelligence*, 2025.

[4] K. Ma, Y. Fu, C. Cao, S. Hou, Y. Huang, and D. Zheng, “Learning visual prompt for gait recognition,” in *CVPR*, 2024, pp. 593–603.

[5] P. Huang, Y. Peng, S. Hou, C. Cao, X. Liu, Z. He, and Y. Huang, “Occluded gait recognition with mixture of experts: An action detection perspective,” in *ECCV*, 2024.

[6] J. Zheng, X. Liu, W. Liu, L. He, C. Yan, and T. Mei, “Gait recognition in the wild with dense 3d representations and a benchmark,” in *CVPR*, 2022, pp. 20228–20237.

[7] Z. Zhu, X. Guo, T. Yang, J. Huang, J. Deng, G. Huang, D. Du, J. Lu, and J. Zhou, “Gait recognition in the wild: A benchmark,” in *ICCV*, 2021, pp. 14 789–14 799.

[8] S. Yu, D. Tan, and T. Tan, “A framework for evaluating the effect of view angle, clothing and carrying condition on gait recognition,” in *ICPR*, vol. 4, 2006, pp. 441–444.

[9] N. Takemura, Y. Makihara, D. Muramatsu, T. Echigo, and Y. Yagi, “Multi-view large population gait dataset and its performance evaluation for cross-view gait recognition,” *IP SJ transactions on Computer Vision and Applications*, vol. 10, pp. 1–14, 2018.

[10] W. Li, S. Hou, C. Zhang, C. Cao, X. Liu, Y. Huang, and Y. Zhao, “An in-depth exploration of person re-identification and gait recognition in cloth-changing conditions,” in *CVPR*, 2023, pp. 13 824–13 833.

[11] C. Shen, C. Fan, W. Wu, R. Wang, G. Q. Huang, and S. Yu, “LidarGait: Benchmarking 3d gait recognition with point clouds,” in *CVPR*, 2023, pp. 1054–1063.

[12] H. Chao, Y. He, J. Zhang, and J. Feng, “GaitSet: Regarding gait as a set for cross-view gait recognition,” in *AAAI*, vol. 33, no. 01, 2019, pp. 8126–8133.

[13] C. Fan, Y. Peng, C. Cao, X. Liu, S. Hou, J. Chi, Y. Huang, Q. Li, and Z. He, “GaitPart: Temporal part-based model for gait recognition,” in *CVPR*, 2020, pp. 14 225–14 233.

[14] B. Lin, S. Zhang, and X. Yu, “Gait recognition via effective global-local feature representation and local temporal aggregation,” in *ICCV*, 2021, pp. 14 648–14 656.

[15] C. Fan, J. Liang, C. Shen, S. Hou, Y. Huang, and S. Yu, “OpenGait: Revisiting gait recognition towards better practicality,” in *CVPR*, 2023, pp. 9707–9716.

[16] M. Wang, X. Guo, B. Lin, T. Yang, Z. Zhu, L. Li, S. Zhang, and X. Yu, “Dygait: Exploiting dynamic representations for high-performance gait recognition,” in *ICCV*, 2023, pp. 13 424–13 433.

[17] H. Dou, P. Zhang, W. Su, Y. Yu, Y. Lin, and X. Li, “GaitGCI: Generative counterfactual intervention for gait recognition,” in *CVPR*, 2023, pp. 5578–5588.

[18] L. Wang, B. Liu, F. Liang, and B. Wang, “Hierarchical spatio-temporal representation learning for gait recognition,” in *ICCV*, 2023, pp. 19 639–19 649.

[19] H. Xiong, B. Feng, X. Wang, and L. Wenyu, “Causality-inspired discriminative feature learning in triple domains for gait recognition,” in *ECCV*, 2024.

[20] Y. Fu, S. Meng, S. Hou, X. Hu, and Y. Huang, “GPGait: Generalized pose-based gait recognition,” in *ICCV*, 2023, pp. 19 595–19 604.

[21] C. Fan, J. Ma, D. Jin, C. Shen, and S. Yu, “Skeletongait: Gait recognition using skeleton maps,” in *AAAI*, vol. 38, no. 2, 2024, pp. 1662–1669.

[22] H. Guo and Q. Ji, “Physics-augmented autoencoder for 3d skeleton-based gait recognition,” in *ICCV*, 2023, pp. 19 627–19 638.

[23] T. Teepe, J. Gilg, F. Herzog, S. Hörmann, and G. Rigoll, “Towards a deeper understanding of skeleton-based gait recognition,” in *CVPR*, 2022, pp. 1569–1577.

[24] H. Zhu, Z. Zheng, and R. Nevatia, “Gait recognition using 3d human body shape inference,” in *WACV*, 2023, pp. 909–918.

[25] X. Han, Y. Ren, P. Cong, Y. Sun, J. Wang, L. Xu, and Y. Ma, “Gait recognition in large-scale free environment via single lidar,” in *ACM MM*, 2024, p. 380–389.

[26] B. Huang, Y. Luo, X. Guo, X. Zheng, Z. Zhu, J. Pan, and C. Zhou, “Watch where you move: Region-aware dynamic aggregation and excitation for gait recognition,” *IEEE Transactions on Multimedia*, 2025.

[27] R. Wang, Y. Shi, H. Ling, Z. Li, C. Zhao, B. Wei, H. Li, and P. Li, “Gait recognition with multi-level skeleton-guided refinement,” *IEEE Transactions on Multimedia*, vol. 26, pp. 4515–4526, 2023.

[28] N. Li and X. Zhao, “A strong and robust skeleton-based gait recognition method with gait periodicity priors,” *IEEE Transactions on Multimedia*, vol. 25, pp. 3046–3058, 2022.

[29] S. Hou, C. Cao, X. Liu, and Y. Huang, “Gait lateral network: Learning discriminative and compact representations for gait recognition,” in *ECCV*, 2020, pp. 382–398.

[30] Z. Wang, S. Hou, M. Zhang, X. Liu, C. Cao, and Y. Huang, “GaitPars: Human semantic parsing for gait recognition,” *IEEE Transactions on Multimedia*, 2023.

[31] J. Zheng, X. Liu, S. Wang, L. Wang, C. Yan, and W. Liu, “Parsing is all you need for accurate gait recognition in the wild,” in *ACM MM*, 2023, pp. 116–124.

[32] J. Liang, C. Fan, S. Hou, C. Shen, Y. Huang, and S. Yu, “Gaitedge: Beyond plain end-to-end gait recognition for better practicality,” in *ECCV*, 2022, pp. 375–390.

[33] D. Ye, C. Fan, J. Ma, X. Liu, and S. Yu, “BigGait: Learning gait representation you want by large vision models,” in *CVPR*, 2024, pp. 200–210.

[34] Z. Wang, S. Hou, M. Zhang, X. Liu, C. Cao, Y. Huang, P. Li, and S. Xu, “QAGait: Revisit gait recognition from a quality perspective,” in *AAAI*, vol. 38, no. 6, 2024, pp. 5785–5793.

[35] L. Wang, Y. Ma, P. Luan, W. Yao, C. Li, and B. Liu, “Hih: A multi-modal hierarchy in hierarchy network for unconstrained gait recognition,” *arXiv preprint arXiv:2311.11210*, 2023.

[36] J. Wang, S. Hou, Y. Huang, C. Cao, X. Liu, Y. Huang, and L. Wang, “Free lunch for gait recognition: A novel relation descriptor,” in *ECCV*, 2024.

[37] D. Ye, C. Fan, Z. Huang, C. Luo, J. Li, S. Yu, and X. Liu, “Biggergait: Unlocking gait recognition with layer-wise representations from large vision models,” *arXiv preprint arXiv:2505.18132*, 2025.

[38] H. Qin, Z. Chen, Q. Guo, Q. J. Wu, and M. Lu, “Rpnet: Gait recognition with relationships between each body-parts,” *IEEE Transactions on Circuits and Systems for Video Technology*, vol. 32, no. 5, pp. 2990–3000, 2021.

[39] J. Wang, S. Hou, X. Guo, Y. Huang, Y. Huang, T. Zhang, and L. Wang, “Gaitc 3 i: Robust cross-covariate gait recognition via causal intervention,” *IEEE Transactions on Circuits and Systems for Video Technology*, 2025.

[40] C. Xu, Y. Makihara, X. Li, Y. Yagi, and J. Lu, “Cross-view gait recognition using pairwise spatial transformer networks,” *IEEE Transactions on Circuits and Systems for Video Technology*, vol. 31, no. 1, pp. 260–274, 2020.

[41] T. Huang, X. Ben, C. Gong, B. Zhang, R. Yan, and Q. Wu, “Enhanced spatial-temporal salience for cross-view gait recognition,” *IEEE Transactions on Circuits and Systems for Video Technology*, vol. 32, no. 10, pp. 6967–6980, 2022.

[42] L. Yao, W. Kusakunniran, Q. Wu, J. Xu, and J. Zhang, “Collaborative feature learning for gait recognition under cloth changes,” vol. 32, no. 6, pp. 3615–3629, 2021.

[43] T. Huang, X. Ben, C. Gong, W. Xu, Q. Wu, and H. Zhou, “Gaitdan: Cross-view gait recognition via adversarial domain adaptation,” *IEEE Transactions on Circuits and Systems for Video Technology*, vol. 34, no. 9, pp. 8026–8040, 2024.

[44] L. Chen, Z. Zhang, and Y. Wang, “Edinogait: Transferring large visual models to event-based vision for enhancing gait recognition,” *IEEE Transactions on Multimedia*, 2025.

[45] S. Zhang, J. Zheng, S. Zhu, and C. Yan, “Trackletgait: A robust framework for gait recognition in the wild,” *IEEE Transactions on Multimedia*, 2025.

[46] S. Hou, X. Liu, C. Cao, and Y. Huang, “Set residual network for silhouette-based gait recognition,” *IEEE Transactions on Biometrics, Behavior, and Identity Science*, vol. 3, no. 3, pp. 384–393, 2021.

[47] G. Peng, Y. Wang, Y. Zhao, S. Zhang, and A. Li, “Glgait: A global-local temporal receptive field network for gait recognition in the wild,” in *ACM MM*, 2024.

[48] Z. Wang, S. Hou, J. Li, X. Liu, C. Cao, Y. Huang, S. Wang, and M. Zhang, “Gait-x: Exploring x modality for generalized gait recognition,” in *ICCV*, 2025, pp. 13 259–13 269.

[49] S. Li, W. Liu, and H. Ma, “Attentive spatial-temporal summary networks for feature learning in irregular gait recognition,” *IEEE Transactions on Multimedia*, vol. 21, no. 9, pp. 2361–2375, 2019.

[50] X. Huang, D. Zhu, H. Wang, X. Wang, B. Yang, B. He, W. Liu, and B. Feng, “Context-sensitive temporal feature learning for gait recognition,” in *ICCV*, 2021, pp. 12 909–12 918.

[51] K. Ma, Y. Fu, D. Zheng, C. Cao, X. Hu, and Y. Huang, “Dynamic aggregated network for gait recognition,” in *CVPR*, 2023, pp. 22 076–22 085.

[52] P. Huang, S. Hou, J. Huang, and Y. Huang, “Learning a unified template for gait recognition,” in *Proceedings of the IEEE/CVF International Conference on Computer Vision*, 2025, pp. 12 459–12 469.

[53] S. Yang, J. Wang, S. Hou, X. Liu, C. Cao, L. Wang, and Y. Huang, “Bridging gait recognition and large language models sequence modeling,” in *CVPR*, 2025, pp. 3460–3469.

[54] M. Deng, Z. Fan, P. Lin, and X. Feng, “Human gait recognition based on frontal-view sequences using gait dynamics and deep learning,” *IEEE Transactions on Multimedia*, vol. 26, pp. 117–126, 2023.

[55] M. Ye, J. Shen, G. Lin, T. Xiang, L. Shao, and S. C. Hoi, “Deep learning for person re-identification: A survey and outlook,” *IEEE Transactions on Pattern Analysis and Machine Intelligence*, vol. 44, no. 6, pp. 2872–2893, 2021.

[56] J. Deng, W. Dong, R. Socher, L.-J. Li, K. Li, and L. Fei-Fei, “Imagenet: A large-scale hierarchical image database,” in *CVPR*, 2009, pp. 248–255.

[57] L. Taylor and G. Nitschke, “Improving deep learning with generic data augmentation,” in *2018 IEEE symposium series on computational intelligence (SSCI)*, 2018, pp. 1542–1547.

[58] B. Zoph, E. D. Cubuk, G. Ghiasi, T.-Y. Lin, J. Shlens, and Q. V. Le, “Learning data augmentation strategies for object detection,” in *ECCV*, 2020, pp. 566–583.

[59] D. Laptev, N. Savinov, J. M. Buhmann, and M. Pollefeys, “Ti-pooling: Transformation-invariant pooling for feature learning in convolutional neural networks,” in *CVPR*, 2016, pp. 289–297.

[60] R. Zhang, “Making convolutional networks shift-invariant again,” in *ICML*, 2019, pp. 7324–7334.

[61] T. Chen, S. Kornblith, M. Norouzi, and G. Hinton, “A simple framework for contrastive learning of visual representations,” in *ICML*, 2020, pp. 1597–1607.

[62] K. He, H. Fan, Y. Wu, S. Xie, and R. Girshick, “Momentum contrast for unsupervised visual representation learning,” in *CVPR*, 2020, pp. 9729–9738.

[63] M. Weiler, M. Geiger, M. Welling, W. Boomsma, and T. S. Cohen, “3d steerable cnns: Learning rotationally equivariant features in volumetric data,” *NeurIPS*, vol. 31, 2018.

[64] M. Weiler, F. A. Hamprecht, and M. Storath, “Learning steerable filters for rotation equivariant cnns,” in *CVPR*, 2018, pp. 849–858.

[65] M. Weiler and G. Cesa, “General $e(2)$ -equivariant steerable cnns,” *NeurIPS*, vol. 32, 2019.

[66] M. Weiler, P. Forré, E. Verlinde, and M. Welling, *Equivariant and Coordinate Independent Convolutional Networks*, 2023.

[67] W. Wang, J. Liang, and D. Liu, “Learning equivariant segmentation with instance-unique querying,” *NeurIPS*, vol. 35, pp. 12 826–12 840, 2022.

[68] J. Han, J. Ding, N. Xue, and G.-S. Xia, “Redet: A rotation-equivariant detector for aerial object detection,” in *CVPR*, 2021, pp. 2786–2795.

[69] H.-X. Yu, J. Wu, and L. Yi, “Rotationally equivariant 3d object detection,” in *CVPR*, 2022, pp. 1456–1464.

[70] W. R. Scott, *Group Theory*. Courier Corporation, 2012.

[71] T. Cohen and M. Welling, “Group equivariant convolutional networks,” in *ICML*, 2016, pp. 2990–2999.

[72] D. Romero, E. Bekkers, J. Tomczak, and M. Hoogendoorn, “Attentive group equivariant convolutional networks,” in *ICML*, 2020, pp. 8188–8199.

[73] G. Cesa, L. Lang, and M. Weiler, “A program to build $e(n)$ -equivariant steerable cnns,” in *ICLR*, 2022.

[74] R. Wang, R. Walters, and R. Yu, “Approximately equivariant networks for imperfectly symmetric dynamics,” 2022.

[75] Y. Pu, Y. Wang, Z. Xia, Y. Han, Y. Wang, W. Gan, Z. Wang, S. Song, and G. Huang, “Adaptive rotated convolution for rotated object detection,” in *ICCV*, 2023, pp. 6589–6600.

[76] J. Wang, S. Hou, Y. Huang, C. Cao, X. Liu, Y. Huang, and L. Wang, “Causal intervention for sparse-view gait recognition,” in *ACM MM*, 2023, pp. 77–85.

[77] H. Farid and E. P. Simoncelli, “Optimally rotation-equivariant directional derivative kernels,” in *International Conference on Computer Analysis of Images and Patterns*. Springer, 1997, pp. 207–214.

[78] Farid and E. P. Simoncelli, “Differentiation of discrete multidimensional signals,” *IEEE Transactions on Image Processing*, vol. 13, no. 4, pp. 496–508, 2004.

[79] B. Chidester, M. N. Do, and J. Ma, “Rotation equivariance and invariance in convolutional neural networks,” *arXiv preprint arXiv:1805.12301*, 2018.

[80] C. Lee, J. Son, H. Shon, Y. Jeon, and J. Kim, “Fred: Towards a full rotation-equivariance in aerial image object detection,” in *AAAI*, vol. 38, no. 4, 2024, pp. 2883–2891.

[81] L. Chen, L. Gu, D. Zheng, and Y. Fu, “Frequency-adaptive dilated convolution for semantic segmentation,” in *CVPR*, 2024, pp. 3414–3425.

[82] X. Glorot and Y. Bengio, “Understanding the difficulty of training deep feedforward neural networks,” in *AISTATS*, 2010, pp. 249–256.

[83] S. Sharma, S. Sharma, and A. Athaiya, “Activation functions in neural networks,” *Towards Data Sci*, vol. 6, no. 12, pp. 310–316, 2017.

[84] A. Vaswani, N. Shazeer, N. Parmar, J. Uszkoreit, L. Jones, A. N. Gomez, Ł. Kaiser, and I. Polosukhin, “Attention is all you need,” *NeurIPS*, 2017.

[85] C. Zhang, X.-P. Chen, G.-Q. Han, and X.-J. Liu, “Spatial transformer network on skeleton-based gait recognition,” *Expert Systems*, p. e13244, 2023.

[86] C. Fan, S. Hou, J. Wang, Y. Huang, and S. Yu, “Learning gait representation from massive unlabelled walking videos: A benchmark,” *IEEE Transactions on Pattern Analysis and Machine Intelligence*, 2023.

[87] H. Dou, P. Zhang, Y. Zhao, L. Jin, and X. Li, “Clash: Complementary learning with neural architecture search for gait recognition,” *IEEE Transactions on Image Processing*, 2024.

[88] X. Ding, X. Zhang, Y. Zhou, J. Han, G. Ding, and J. Sun, “Scaling up your kernels to 31x31: Revisiting large kernel design in cnns,” in *CVPR*, 2022.